

Late accretion of Ceres-like asteroids and their implantation into the outer main belt

In the format provided by the
authors and unedited

Table of contents

Supplementary Figure 1.....	2
Supplementary Figure 2.....	3
Supplementary Figure 3.....	5
Supplementary Figure 4.....	7
Supplementary Table 1.....	9
Supplementary Table 2.....	9
Supplementary Table 3.....	10
Supplementary Table 4.....	11
Supplementary Table 5.....	11
Supplementary Table 6.....	11
References.....	13

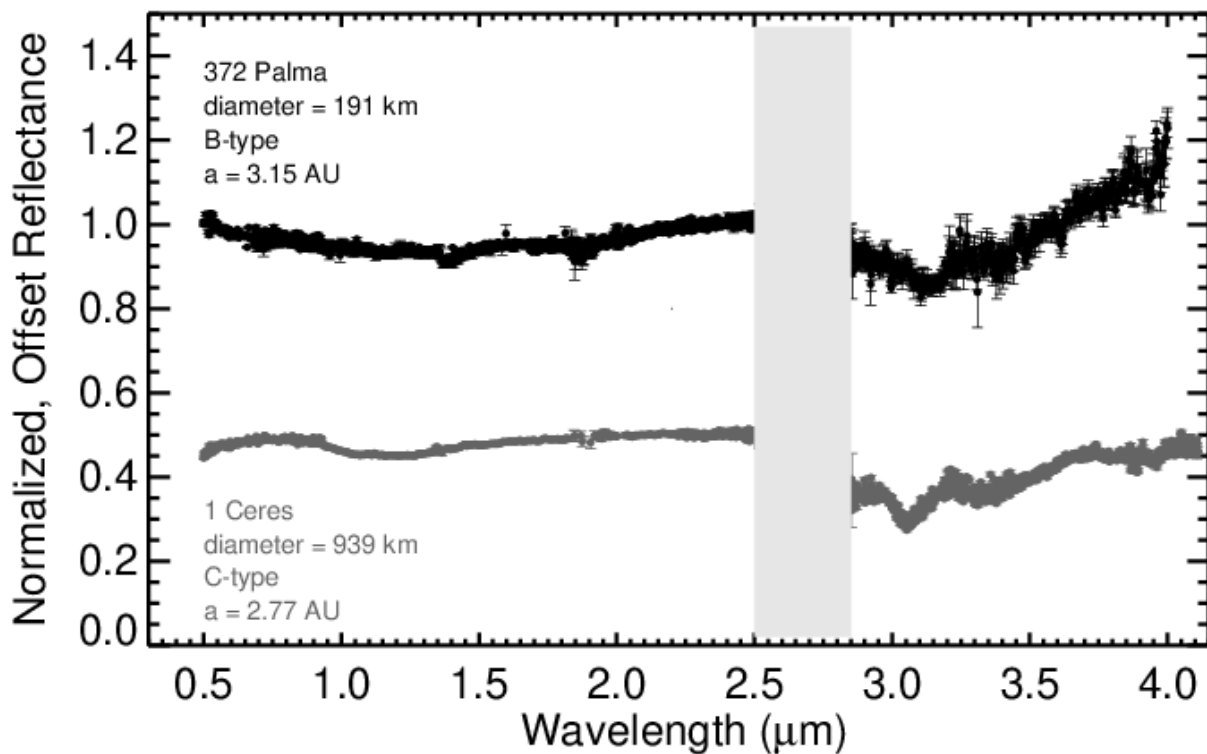
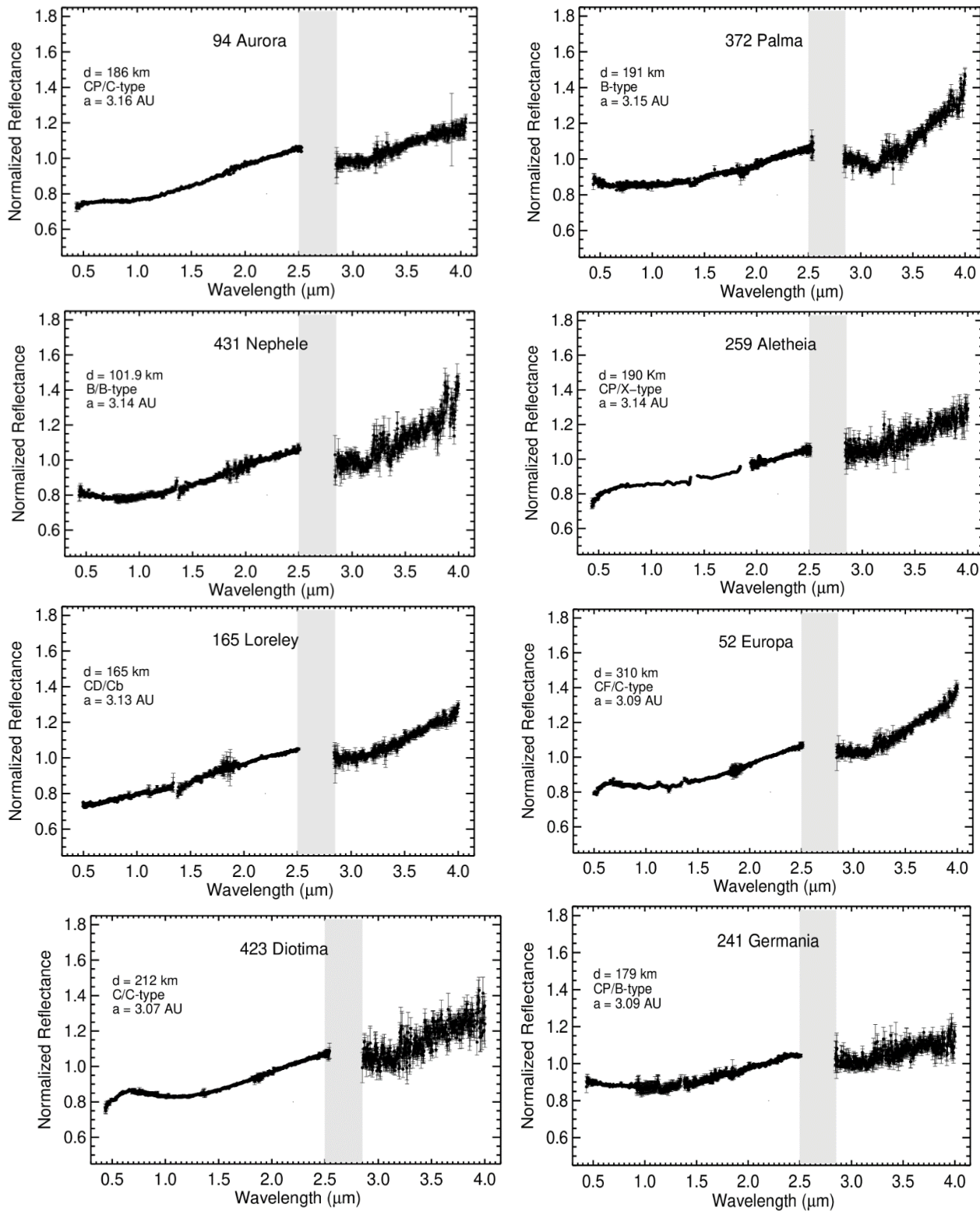


Fig. 1. Near-infrared reflectance spectrum (binned x 6) of asteroid 372 Palma is constant with the dwarf planet 1 Ceres. Palma's spectrum has a broad 1- μm absorption feature and an absorption band centered around 3.15 μm , consistent with Ceres' spectrum ([MITHNEOS MIT-Hawaii Near-Earth Object Spectroscopic Survey](#), (1)). The gray bar marks wavelengths of strong absorption by water vapor in Earth's atmosphere. See Supplementary Fig. 2 for spectra of all other newly identified large dark asteroids. Uncertainties were computed by Spextool software (2) using the Robust Weighted Mean algorithm with a clipping threshold of 8 (sigma). The value at each pixel is the weighted average of the good pixels, and the propagated variance gives the uncertainty.



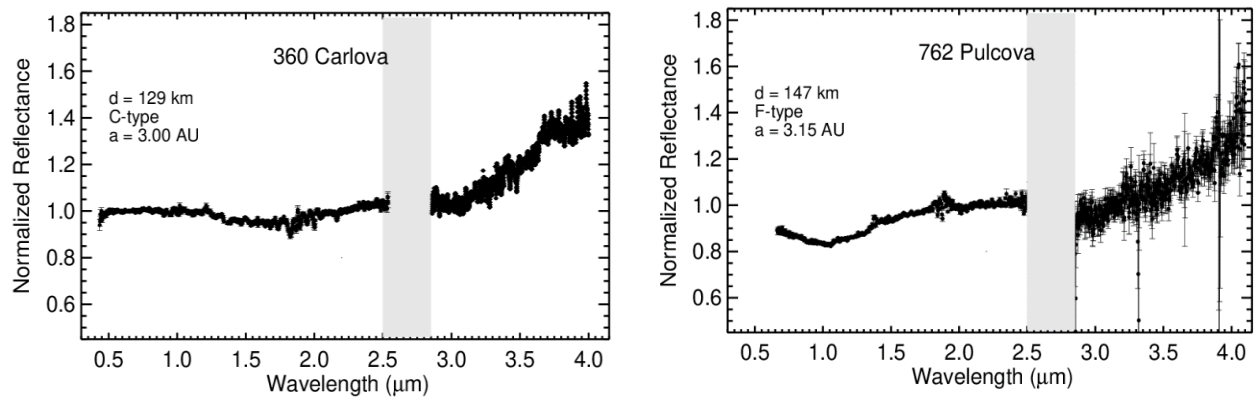
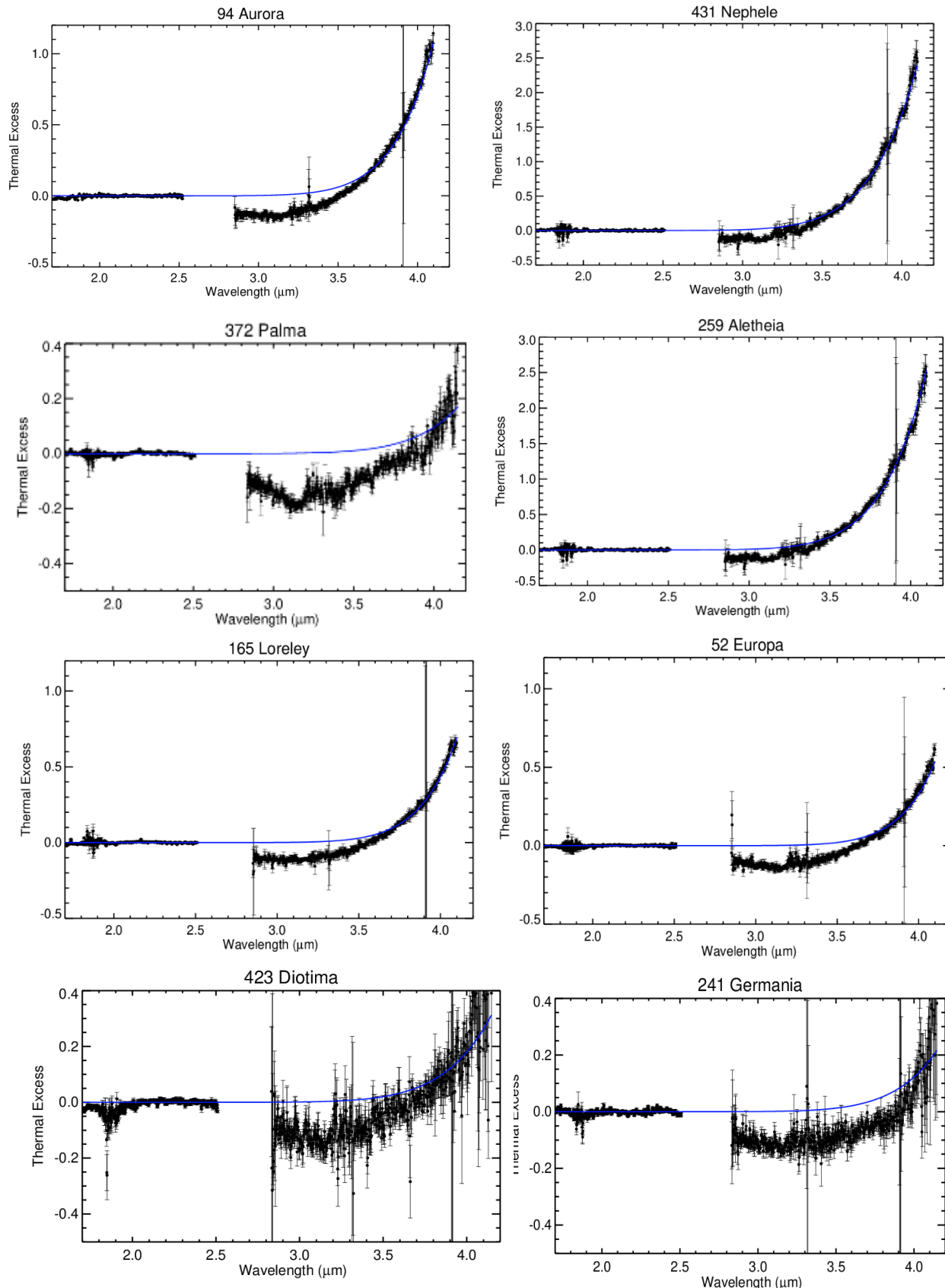


Fig. 2. Near-infrared (binned \times 6) reflectance spectra of newly identified large dark asteroids found to be consistent with the dwarf planet 1 Ceres. All spectra have been normalized to unity at $2.2 \mu\text{m}$. The gray bar on each plot marks wavelengths of strong absorption by water vapor in Earth's atmosphere. Asteroid (52) Europa was reobserved in this study, and its spectra were found to be similar to the ones published in Takir and Emery (3). Uncertainties were computed by Spextool software using the Robust Weighted Mean algorithm with a clipping threshold of 8 (sigma). The value at each pixel is the weighted average of the good pixels, and the propagated variance gives the uncertainty.



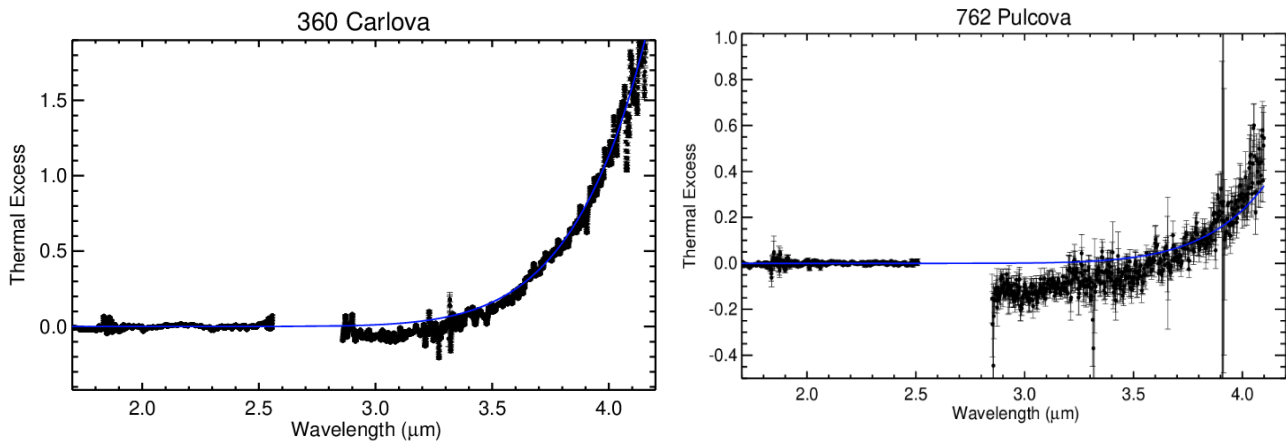
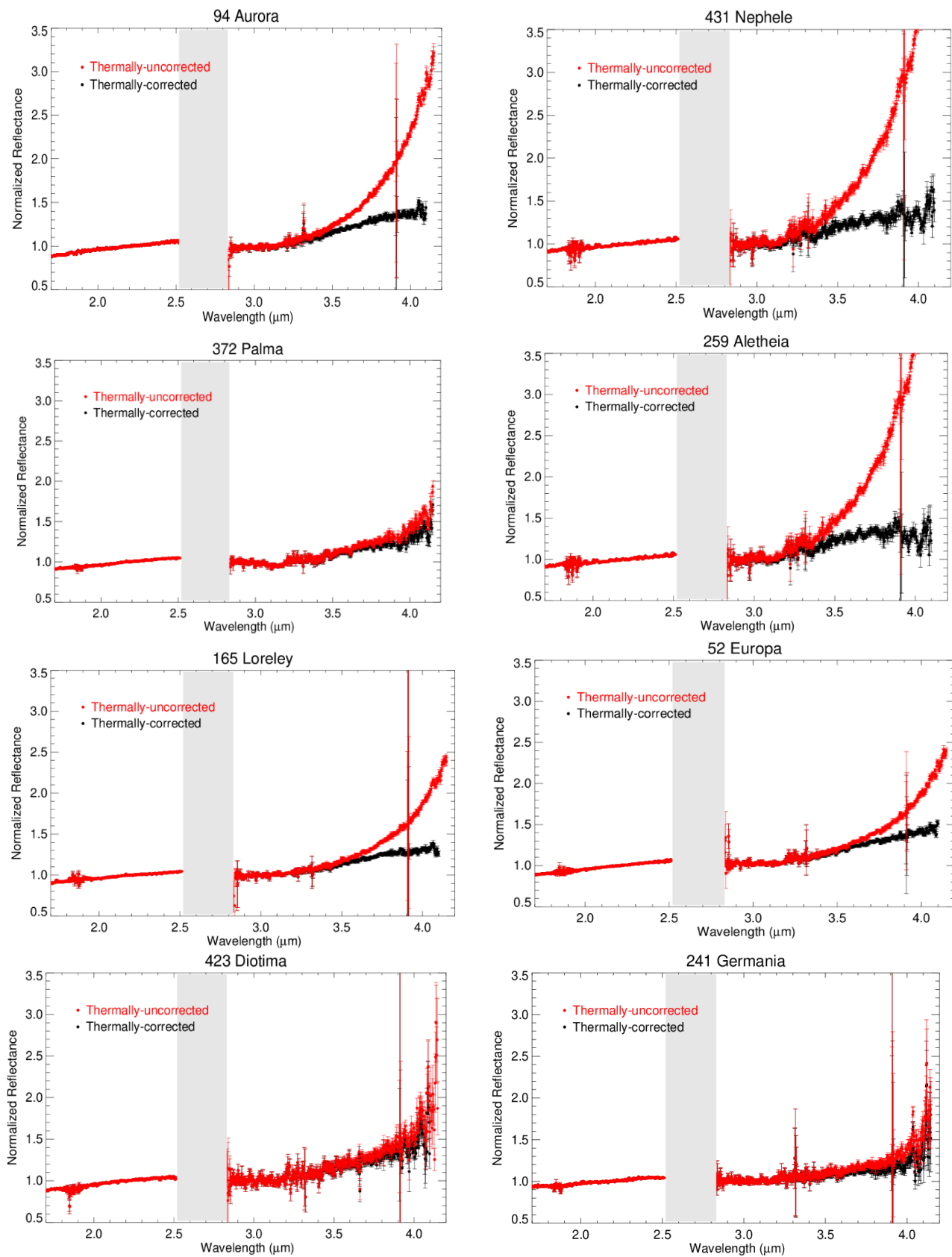


Fig. 3. Thermal excess and NEATM’s best thermal model (in blue) for the studied large dark asteroids. Uncertainties were computed by Spextool software using the Robust Weighted Mean algorithm with a clipping threshold of 8 (sigma). The value at each pixel is the weighted average of the good pixels, and the propagated variance gives the uncertainty.



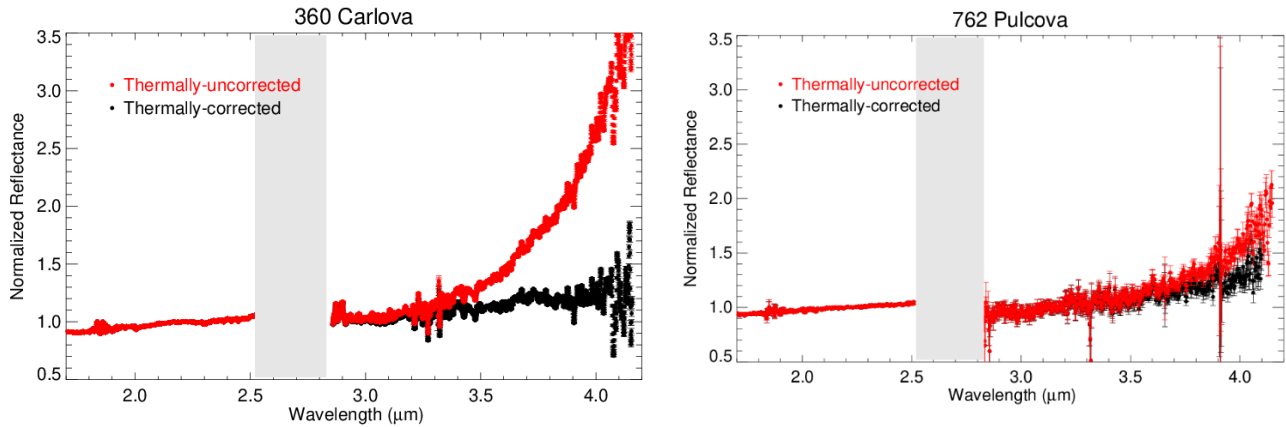


Fig. 4. Thermally uncorrected (red) and corrected (black) spectra of large dark asteroids.
 The gray bar marks wavelengths of strong absorption by water vapor in Earth's atmosphere.
 Uncertainties were computed by Spextool software using the Robust Weighted Mean algorithm
 with a clipping threshold of 8 (sigma). The value at each pixel is the weighted average of the
 good pixels, and the propagated variance gives the uncertainty.

Table 1. Physical properties of the large dark asteroids included in this study. Source: <http://ssd.jpl.nasa.gov/sbdb.cgi>. Asteroid (65) Cybele was observed by Licandro et al. (4); asteroid 24 Themis was observed by Rivkin and Emery (5) and Campins et al. (6); asteroids 31 Euphrosyne, 10 Hygiea, and 451 Patientia were observed by Takir and Emery (3).

Asteroid	a (AU)	Eccentricity	Inclination (deg)	diameter (km)*	Spectral Class	Albedo	Average Density (kg m ⁻³)*
65 Cybele	3.42	0.11	3.57	248.29 ± 17.59	P/Xc	0.071	1700 ± 520
94 Aurora	3.16	0.09	7.97	186.35 ± 8.84	CP/C	0.040	1830 ± 1100
31 Euphrosyne	3.16	0.22	26.27	272.82 ± 8.85	C	0.054	--
372 Palma	3.15	0.25	23.82	191.12 ± 2.68	BFC/B	0.059	1400 ± 180
431 Nephele	3.14	0.17	1.83	93.00 ± 4.00	B/B	0.055	1767 ± 1007
259 Aletheia	3.14	0.12	10.81	190.05 ± 6.82	CP/X	0.043	2160 ± 260
10 Hygiea	3.14	0.11	3.83	421.60 ± 25.69	C	0.072	1945 ± 265
24 Themis	3.14	0.12	0.75	183.84 ± 11.40	C/B	0.067	1810 ± 670
762 Pulcova	3.15	0.11	13.10	138.40 ± 5.96	F	0.040	1000 ± 140
165 Loreley	3.13	0.09	11.23	164.92 ± 8.14	CD/Cb	0.047	--
52 Europa	3.09	0.11	7.48	310.21 ± 10.34	CF/C	0.057	1500 ± 400
423 Diotima	3.07	0.04	11.24	211.64 ± 16.02	C/C	0.067	1390 ± 500
451 Patientia	3.06	0.07	15.20	234.42 ± 10.17	CU	0.076	1600 ± 800

*The diameter and average density are from Carry (7) and Vernazza et al. (8) as well as Fienga et al. (9).

Table 2. Band depth, center, and area calculations with uncertainties for the studied large dark asteroids. Source: <http://ssd.jpl.nasa.gov/horizons.cgi>. This table also includes asteroid thermal model inputs used for the studied large and dark asteroids.

Asteroid	3-μm Band Center (μm)	3-μm Band Depth (%)	3-μm Band Area (μm ⁻¹)	Rau (AU)	Dau (AU)	Phase (deg)	Abs. Mag.	Rotation Period (h)	K/V*	Temp** (K)
360 Carlova	3.05 ± 0.06	5.68 ± 0.43	0.012 ± 0.003	2.51	1.59	9.65	8.56	6.18	0.99	253.4
241 Germania	3.11 ± 0.03	3.79 ± 0.74	0.010 ± 0.005	3.34	2.41	6.72	7.78	15.51	0.82	86.9
423 Diotima	3.12 ± 0.01	5.93 0.86	0.015 ± 0.006	3.18	2.28	8.74	7.34	4.77	1.37	151.7
52 Europa	3.15 ± 0.01	3.89 ± 0.62	0.008 ± 0.004	2.89	3.22	18.09	6.48	5.63	1.22	228.2
762 Pulcova	3.01 ± 0.01	6.12 ± 0.65	0.011 ± 0.005	3.26	2.33	7.70	8.04	5.84	1.05	222.48
165 Loreley	3.07 ± 0.04	1.94 ± 0.47	0.006 ± 0.005	2.90	1.90	3.15	7.88	7.23	1.33	180.5
431 Nephele	3.13 ± 0.01	7.48 ± 0.57	0.014 ± 0.003	3.14	2.60	1.60	8.94	13.53	1.27	228.1

259 Aletheia	3.13±0.01	3.98±0.26	0.009±0.002	3.52	2.55	3.20	7.90	8.14	1.23	215.5
372 Palma	3.13±0.01	7.48±0.57	0.014±0.003	3.22	2.22	2.02	7.46	8.57	1.16	173.1
94 Aurora	3.13±0.01	3.43±0.37	0.006±0.002	2.97	2.99	19.19	7.66	7.22	1.35	197.3

* K-band to V-band scale, applied to spectra to reconcile the two reflectance values at two different wavelengths. Rau is the heliocentric range, and Dau is the geocentric range.

** Temperatures corresponding to optimum thermal models.

Table 3. Key properties of asteroids fitted with thermal evolution models (columns 2-7), initial diameters (column 8), intermediate (columns 9-11), and final (columns 13-17) properties of asteroid fits, as well as the accretion times derived. Intermediate objects are slightly larger than the final objects since they have a non-hydrated and non-lithified surface layer of less than a few 100 m. After losing this thin layer by impacts, slightly smaller objects that reproduce the observed properties of asteroids are obtained. The current porosities were calculated from the masses and volumes (7, 8, 9) assuming a CM-like grain density of 2460 kg m⁻³ for all asteroids based on their spectral similarity and meteorite analogues provided in Carry et al. (7). Note that Carry et al. (7) assumed rubble pile structures and neglected the microporosity, while we provide the total porosity in the table. The theoretical reference diameters are diameters at zero porosity. The initial bulk density is 1230 kg m⁻³, and the initial porosity is 50% for all objects. The accretion times derived include uncertainties for those cases for which they could be estimated.

Asteroid	Current semi-major axis	Current bulk density	Current porosity	Current diameter	Ref. diameter	Ref. mass	Fit initial diameter	Fit intermediate density	Fit intermediate porosity	Fit intermediate diameter	Fit final density	Fit final porosity	Fit final diameter	Fit ref. diameter	Fit ref. mass	Derived accretion time
	AU	kg m ⁻³	%	km	km	kg	km	kg m ⁻³	%	km	kg m ⁻³	%	km	km	kg	Ma
10 Hygiea	3.14	1945±265	21	434	401.3	8,31E+19	506.5	1941	21.1	435.0	1946	20.9	434	402	8,37E+19	2.65 -0.7
24 Themis	3.14	1810±670	26	183.8	166	5,89E+18	209	1795	27.0	184.5	1800	26.8	184	166	5,89E+18	1.69
52 Europa	2.89	1500±400	38	310.2	264.4	2,38E+19	335	1519	38.3	312.4	1520	38.2	310.4	266	2,42E+19	3.2 -1.5
65 Cybele	3.43	1700±520	31	248.3	219.4	1,36E+19	277	1706	30.7	248.6	1709	30.5	248	220	1,37E+19	1.8 -0.4
94 Aurora	2.97	1830±1100	26	186.4	169.1	6,23E+18	214	1827	25.7	187.7	1831	25.6	187.2	170	6,33E+18	1.68
259 Aletheia	3.52	2160±260	12	190.1	182.2	7,79E+18	229	2169	11.2	190.5	2176	11.5	190	182	7,77E+18	1.55 +0.1/-0.6
372 Palma	3.22	1400±180	43	191.1	158.7	5,15E+18	201	1425	42.1	191.9	1427	42	191.2	160	5,28E+18	2 -0.1
423 Diotima	3.18	1390±500	43	211.6	175.1	6,91E+18	222	1398	43.2	212.5	1400	43.1	211.6	176	7,02E+18	2.25 -0.6
431 Nephele	3.14	1767±1007	28.2	93	83.3	7,45E+17	106	1771	28	93.7	1777	27.7	93.3	84	7,63E+17	1.57
451 Patientia	3.06	1600±800	35	234.4	203.8	1,09E+19	257	1610	34.6	235	1613	34.4	234.4	204	1,09E+19	1.86 -0.9

Table 4. Observing parameters for asteroids observed in this study with the LXD mode of SpeX at NASA IRTF.

Asteroid	Date (UT)	Time (UT)	Airmass	Standard star	Spectral type	B-V*	V-K*
94 Aurora	10/28/19	12:51-15:31	1.19-2.84	SAO 75554	G0	0.63	1.66
372 Palma	08/21/16	11:12-13:13	1.13-1.44	HD 210105	G2V	0.62	1.50
431 Nephele	02/09/18	8:30-12:35	1.34-1.33	HD 217196	G5V	0.69	1.62
259 Aletheia	11/13/16	9:06-9:20	1.14-1.12	HD285597	G0	0.68	1.61
762 Pulcova	09/9/20	8:41-11:00	1.17-1.01	SAO_74411	G5	0.67	1.58
165 Loreley	08/11/20	11:50-14:45	1.17-1.88	HD 207094	G2V	0.63	1.41
52 Europa	06/22/17	5:51-7:19	1.23-1.13	HD 133584	G1V	--	--
423 Diotima	12/16/15	12:43-13:09	1.01-1.04	SAO 79579	G5	0.64	1.46
241 Germania	02/04/20	13:20-16:10	1.13-2.39	SAO 118200	G5	0.71	1.86
360 Carlova	01/04/17	5:32-7:38	1.52-1.06	HD 244686	G0	0.66	1.55

*B-V and V-K represent stars' colors.

Table 5. Observing parameters for asteroids observed in this study with the Prism mode of SpeX at NASA IRTF. The prism spectrum of asteroid 762 Pulcova is from (10).

Asteroid	Date (UT)	Time (UT)	Airmass	Standard star	Spectral type	B-V	V-K
94 Aurora	12/29/20	14:04-14:50	1.00-1.03	HD 86043	G5	0.60	1.41
372 Palma	08/21/16	13:33-13:40	1.59-1.60	HD 210105	G2V	0.62	1.50
431 Nephele	12/29/20	10:03-12:07	1.10-1.29	SAO 98993	G0	0.63	1.59
259 Aletheia	11/13/16	7:56-8:10	1.40-1.43	HD 285597	G0	0.68	1.61
165 Loreley	12/29/20	4.53-5.37	1.46-1.38	HD 211567	G5V	0.61	1.46
52 Europa	12/29/20	6.25-7.34	1.82-1.60	HD 258906	G5	0.66	1.54
423 Diotima	12/29/20	5:41-6.31	1.38-1.83	HD 283933	G0	0.62	1.62
241 Germania	12/29/20	14:54-15:54	1.94-1.51	HD 123715	G3V	0.64	1.52
360 Carlova	01/04/17	8:40-8:48	1.01-1.01	HD244686	G0	0.66	1.55

*B-V and *V-K represent stars' colors.

Table 6: Parameters used for the calculation of radiogenic energy. Heat Sources: The element mass fractions are referenced in Eq 1. The element mass fractions refer to stable isotopes, the initial ratios are between unstable and stable isotopes of an element, and the decay energies are per particle. The number of atoms of the stable isotope per 1 kg of the primordial material is

$f=xN_A/m_a$ with the relative mass fraction x of the stable isotope, the molar mass of the radioactive isotope m_a in kg, and the Avogadro number N_A .

Isotope	^{26}Al	^{60}Fe	^{40}K	^{232}Th	^{235}U	^{238}U
Element mass fraction x	$8.68 \cdot 10^{-3}$	$1.81 \cdot 10^{-1}$	$5.32 \cdot 10^{-4}$	$2.96 \cdot 10^{-8}$	$8.08 \cdot 10^{-9}$	$8.08 \cdot 10^{-9}$
Half-life λ [years]	$7.17 \cdot 10^5$	$2.62 \cdot 10^6$	$1.25 \cdot 10^9$	$1.41 \cdot 10^{10}$	$7.04 \cdot 10^8$	$4.47 \cdot 10^9$
Initial ratio Z	$5 \cdot 10^{-5}$	$1.15 \cdot 10^{-8}$	$1.50 \cdot 10^{-3}$	1.0	$8 \cdot 10^{-3}$	$9.92 \cdot 10^{-1}$
Decay energy E [J]	$4.99 \cdot 10^{-13}$	$4.34 \cdot 10^{-13}$	$1.11 \cdot 10^{-13}$	$6.47 \cdot 10^{-12}$	$7.11 \cdot 10^{-13}$	$7.61 \cdot 10^{-12}$

References

1. Rivkin, A.S., Howell, E.S., Emery, J.P., Infrared Spectroscopy of Large, Low-Albedo Asteroids: Are Ceres and Themis Archetypes or Outliers? *Journal of Geophysical Research: Planets* **124**, Issue 5 p. 1393-1409 (2019).
2. Cushing, M. Spectral Extraction Package for SpeX, a 0.8-5.5 Micron Cross-Dispersed Spectrograph. *The Astronomical Society of the Pacific* **166**, 362-376 (2004).
3. Takir, D. & Emery, J.P. Outer Main Belt asteroids: Identification and distribution of four 3- μm spectral groups. *Icarus* **219**, 641-654 (2012).
4. Licandro, L. et al. 65 Cybele: Detection of small silicate grains, water-ice and organics. *Astronomy. Astrophysics.* **525**, A34 (2011).
5. Rivkin, A.S., Emery, J.P., Detection of ice and organics on an asteroidal surface. *Nature* **64**, 1322–1323 (2010).
6. Campins, H. et al., Water ice and organics on the surface of the Asteroid 24 Themis. *Nature* **464**, 1320–1321(2010).
7. Carry, B. Density of asteroids. *Planetary and Space Science* **73** 98-118 (2012).
8. Vernazza, P. et al. A basin-free spherical shape as an outcome of a giant impact on asteroid Hygiea. *Nature Astronomy* **4**, 136–141 (2020).
9. A Fienga, A., Avdellidou, C., Hanuš, J. Asteroid masses obtained with INPOP planetary ephemerides. *Monthly Notices of the Royal Astronomical Society* **492**(1), 589–602 (2020).
10. Lindsay, S.S., Marchis, F., Emery, J.P., Enriquez, J.E., Assafin, M. Composition, mineralogy, and porosity of multiple asteroid systems from visible and near-infrared spectral data. *Icarus* **247**, 53-70 (2015).